Bioactive Materials 9 (2022) 134–146

Contents lists available at ScienceDirect

Bioactive Materials

journal homepage: www.sciencedirect.com/journal/bioactive-materials

Micropatterns and peptide gradient on the inner surface of a guidance conduit synergistically promotes nerve regeneration *in vivo*

Deteng Zhang [a,b], Ziming Li [a], Haifei Shi [c], Yuejun Yao [a], Wang Du [a], Pan Lu [c], Kejiong Liang [c], Liangjie Hong [a], Changyou Gao [a,b,*]

[a] *MOE Key Laboratory of Macromolecular Synthesis and Functionalization, Department of Polymer Science and Engineering, Zhejiang University, Hangzhou, 310027, China*

[b] *Dr. Li Dak Sum & Yip Yio Chin Center for Stem Cell and Regenerative Medicine, Zhejiang University, Hangzhou, 310058, China*

[c] *Department of Hand Surgery, First Affiliated Hospital of Zhejiang University, School of Medicine. Hangzhou, 310009, China*

ARTICLE INFO

Keywords:
Peptides gradient
Micropatterns
Contact guidance effect
Nerve guidance conduits
Nerve regeneration

ABSTRACT

Both of the surface topographical features and distribution of biochemical cues can influence the cell-substrate interactions and thereby tissue regeneration *in vivo*. However, they have not been combined simultaneously onto a biodegradable scaffold to demonstrate the synergistic role so far. In this study, a proof-of-concept study is performed to prepare micropatterns and peptide gradient on the inner wall of a poly (D,L-lactide-*co*-caprolactone) (PLCL) guidance conduit and its advantages in regeneration of peripheral nerve *in vivo*. After linear ridges/grooves of 20/40 μm in width are created on the PLCL film, its surface is aminolyzed in a kinetically controlled manner to obtain the continuous gradient of amino groups, which are then transferred to CQAASIKVAV peptide density gradient via covalent coupling of glutaraldehyde. The Schwann cells are better aligned along with the stripes, and show a faster migration rate toward the region of higher peptide density. Implantation of the nerve guidance conduit made of the PLCL film having both the micropatterns and peptide gradient can significantly accelerate the regeneration of sciatic nerve in terms of rate, function recovery and microstructures, and reduction of fibrosis in muscle tissues. Moreover, this nerve conduit can also benefit the M2 polarization of macrophages and promote vascularization *in vivo*.

1. Introduction

The surface physiochemical and geometrical properties of implantable biomaterials strongly mediate cell-substrate interactions, and thereby influence the regeneration and remodeling processes of tissues. The biomaterials surface having specific microstructures and biochemical cues can maximally mimic the extracellular matrix (ECM), which provides a temporary structural and signal platform that promotes proliferation, polarization, differentiation, and organization of cells to form tissue microarchitecture with appropriate biological functions [1]. The micropatterns that can effectively elaborate cell spatial arrangement have caused increasing attention. For instance, manipulating drug-laden poly (lactic-*co*-glycolic acid) (PLGA) into microgrooves using Teflon stamps is a promising method for repairing tendon injury [2]. The micropatterned fibronectin substrates can guide the adhesion and growth of lung fibroblasts to form the oriented fibroblast-derived matrix, which promotes the directional tubulogenesis [3].

On the other hand, abundant biophysical and biochemical cues of native ECM often exist along with spatial and temporal gradients, which afford for the spatially diverse functional requirements such as inflammatory response, development and morphogenesis, reproductive biology, tissue structuring and organization, and many disease processes [4]. Indeed, cells in a native tissue are usually exposed to complex gradient signals, which are derived from their specific surrounding ECM including architectural structure, mechanical properties, as well as chemical compositions including proteins, growth factors and chemokines [5]. For example, tumor cells are sensitive to the oxygen concentration gradient and pH gradient, and prefer to migrate toward the direction of abundant blood vessels, which is a vital key to tumor metastasis [6]. Inversely, endothelial cells are inclined to migrate

Peer review under responsibility of KeAi Communications Co., Ltd.

* Corresponding author. MOE Key Laboratory of Macromolecular Synthesis and Functionalization, Department of Polymer Science and Engineering, Zhejiang University, Hangzhou, 310027, China.

E-mail address: cygao@zju.edu.cn (C. Gao).

https://doi.org/10.1016/j.bioactmat.2021.07.010
Received 8 May 2021; Received in revised form 9 July 2021; Accepted 10 July 2021
Available online 15 July 2021

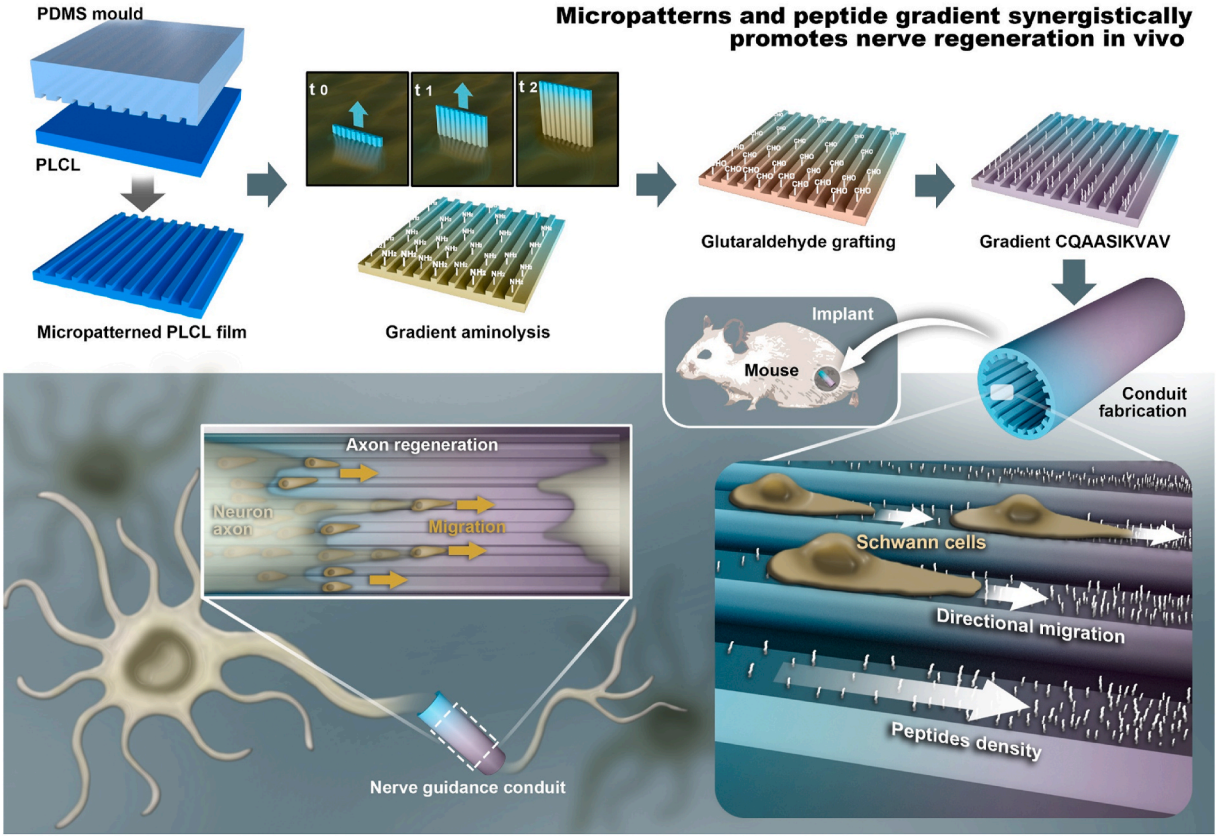

Scheme 1. Schematic drawing to delineate the preparation of micropatterned poly (D,L-lactide-*co*-caprolactone) (PLCL) film incorporated with a CQAASIKVAV peptide density gradient, which is manufactured into conduit for peripheral nerve regeneration. The stripe micropatterns with ridges and grooves are fabricated via polydimethylsiloxane (PDMS) template thermally pressing onto a PLCL film, which is then aminolyzed in 1,6-hexanediamine solution via a time-controlled injection method to obtain the gradient distribution of amino groups along the stripes. By covalent coupling with GA, the density gradient of amino group is transferred to the CQAASIKVAV peptides density gradient. The micropatterned PLCL film with a peptide gradient can synergistically enhance the directional migration of SCs toward to the high density region of the patterns *in vitro*, whereas the guidance conduit obtained thereof can significantly promote the reconstruction and functional recovery of rat sciatic nerve *in vivo*.

toward the lower value of an extracellular pH gradient due to the increase of protrusion stability and actin-integrin adhesion complex formation on cell membrane, which could benefit to the cellular favorable polarization and directional migration [7].

Therefore, gradient biomaterials or scaffolds with anisotropic features such as compositions (e.g., different polymer compositions or concentrations), surface structures (e.g., surface patterns, polymer thickness, pore size or porosity), mechanical properties (e.g., modulus, wettability, crystallinity or stiffness), anchored biomolecules (e.g., proteins or peptides) or loaded factors (e.g., nerve growth factor (NGF)) are key regulators for the behaviors of cells *in vivo*, which respond to the complex nature of the ECM environment during tissue regeneration process [8–10]. For instance, the amount of adsorbed protein and subsequent cell adhesion and spreading can be manipulated by changing the poly (ethylene glycol) (PEG) gradient density on titanium dioxide surfaces [9]. In another case, the cell aspect ratio of adipose-derived stem cells shows positive correlation to the underlying linear stiffness gradient hydrogels made of methacryloyl gelatin (GelMA) [11]. In addition, the osteogenic differentiation of human mesenchymal stem cells exhibits a linear correlation with the interfacial roughness gradient surface as a result of high nuclear tension and transcriptional activity [12]. Moreover, mesenchymal stem cells exhibit enhanced migration toward a gradient of stromal cell derived factor-1 (SDF-1), laying the foundation for acute ischemic/reperfusion injury *in vivo* [13]. Hence, gradient degradable biomaterial scaffolds impose great potential and prospect in tissue repair and regenerative medicine.

Large injuries in peripheral nerve system (PNS) that cause sensory and motor severe impairment drastically affect millions of patients' life quality, resulting in major socioeconomic loss [14]. Based on the well-organized microstructures of native nerve fibers in PNS, oriented electrospinning fibers, microchannels and stripes have been used to guide the cell behaviors and nerve regeneration. For example, the neurite length, rate, and orientation of dorsal root ganglia are effectively enhanced by 40 μm width patterns [15]. The directional migration of Schwann cells (SCs) and the extension of neurite are significantly promoted by gelatin, peptide and graphene oxide nanosheets-modified micropatterns on the surface of polyester films [16–18]. On the other hand, plenty efforts have been paid in constructing surfaces with gradient signals of biochemical molecules and/or physical guidance cues to interact with cells and govern their behaviors [19]. For example, a complementary gradient of KHIFSDDSSE peptides and poly (3-dimethyl-methacryloyloxyethyl ammonium propane sulfonate) manipulate effectively the migration direction and migration rate of SCs, whereas reduce the migration rate of competitive fibroblasts [20]. In another study, the neurite length of dorsal root ganglia (DRG) in the middle of the gradient NGF-immobilized film is significantly longer than that on a uniform NGF-immobilized film [21]. Furthermore, the gradient NGF-immobilized nerve guidance conduit achieves morphological and functional improvements of regenerated nerves, which bridged across a 14 mm gap in rats 12 w post implantation [22,23].

Nevertheless, a scaffold having both topography guidance and programmed gradient biological signals have not been reported so far, neither its effects on tissue regeneration *in vivo*. Cells can sense environments such as physical topology and chemical gradient signals, and

adjust their shape and behavior accordingly. It is known that micropatterns have a so-called contact guidance effect, enabling the cells align along with patterns [3]. When the patterns are made in a linear manner, cells will mainly align along with the linear direction, which is important for those types of tissues needing orientation in a direction [17]. On the other hand, the chemical gradient on a substrate can promote migration of cells toward the higher density region of cell-affinitive ligands [20]. Taking together, it is reasonable to assume that the conduit having both the micropatterns and peptide gradient can better promote the peripheral nerve regeneration because of the good cell alignment and unidirectional migration. When the conduit end of higher density of peptides is placed at the distal region, it is supposed that the cells, especially SCs playing an important role for nerve regeneration will preferentially migrate to the distal end with a faster rate, resulting in a faster and better peripheral nerve regeneration.

Herein, regular ridges and grooves in a micron scale are created on a poly (D,L-lactide-*co*-caprolactone) (PLCL) film by a template thermo-pressing method, following with introduction of gradient amino groups along the stripes by a kinetically controlled reaction (Scheme 1). The PLCL film is certificated as biodegradable polymer due to the hydrolysable ester group [16]. The functional CQAASIKVAV peptides derived from laminin are covalently grafted in a gradient manner via glutaraldehyde (GA) coupling. The surface properties of films are well characterized in terms of topography and peptide gradient, and the guidance of SCs migration is assessed. The films are manufactured into NGCs for sciatic nerve regeneration in rats, and the histological and functional recovery of the regenerated nerves is systematically analyzed. Furthermore, the macrophage phenotype and vascular structures are detected by immunohistochemical and immunofluorescence staining. The success of the NGCs having peptide gradient density along the microgrooves in nerve regeneration *in vivo* demonstrates the significance of deliberately designed surface structures.

2. Experimental section

2.1. Materials

PLCL were synthesized from L-lactide and ε-caprolactone with a molar ratio of 50: 50 (Mw 90 kDa) and 75: 25 (Mw 35 kDa) (Jinan Daigang Biotech Co., Ltd., China). Tertiary butanol, trichloromethane, formaldehyde, isopropyl alcohol, GA, acetone, paraformaldehyde and 1,6-hexanediamine were obtained from Sinopharm Chemical Reagent Co., China. Ninhydrin hydrate (98%) and 5,5′-dithiobis-(2-nitrobenzoic acid) (DTNB) were obtained from Macklin Biochemical Co., Ltd. CQAASIKVAV peptides were customized from GL Biochem Ltd., China. Milli-Q water was used for all the experiments (Millipore, USA).

2.2. Preparation and characterization of peptide gradient along micropatterned PLCL films

PLCL (50: 50, 0.7 g) and PLCL (75: 25, 0.3 g) were dissolved in 14 mL trichloromethane and then stirred for 1 day at 25 °C. The prepared homogeneous solution was cast onto an oblong mould made by polytetrafluoroethylene (PTFE). After solvent evaporation naturally, original flat PLCL film was obtained. Next, the flat film was endowed with stripe micropatterns by a "two-step replicating template method". In brief, a PDMS stamp with grooves and ridges of 20/40 μm in width was firstly fabricated from a micropatterned silicon wafer, and then the PDMS stamp was pressed onto the flat PLCL film at 190 °C to obtain the micropatterned PLCL with 40/20 μm in width of groove/ridge. The micropatterned film was then immersed in 5% (v/v) 1,6-hexanediamine/isopropanol solution (named as aminolysis solution) at 37 °C for 1, 2, 3, 4, 6, 8, 10, 12, 14, 16, 18 and 20 min, and then rinsed 6 times with water. The amino groups were then transferred to aldehyde groups by being incubated in 2% (v/v) GA/water solution for 4 h at 37 °C, which were then reacted with CQAASIKVAV (0.4% wt/v) water solution for 4 h at 37 °C to graft the peptides. After washed 6 times with water, the peptides-modified PLCL film was dried under a nitrogen gas flow.

To prepare the micropatterned and gradient peptide film (MG film), the micropatterned film was placed vertically in a self-made vessel, into which the aminolysis solution was carefully injected by a micro-infusion pump (WZS-50F2, Zhejiang University Medical Instrument, China) at 37 °C. According to the results of cell adhesion, the reaction time to form the gradient $-NH_2$ density on the surface was fixed at 8 min. Following the same treatments as described above, the MG film was obtained. The flat film with gradient peptides obtained by the same method was designated as FG film. The micropatterned PLCL film with uniform peptide distribution (4 min aminolysis) was designated as MU film. The flat film without any treatment was designated as Flat film.

The morphology of the films was observed by a scanning electron microscope (SEM, Hitachi S-4800, Japan). The height of the micropatterns was detected using a profilometer (Dektak 150, Veeco, USA). The wettability of the films was measured using a static water contact angle measuring system (Krüss DSA100, Germany). The density distribution of NH_2 groups on the PLCL film was quantitatively measured using a ninhydrin assay method [24]. The peptides-grafted film was reacted with 5,5′-dithiobis-(2-nitrobenzoic acid) (DTNB, an Ellman reagent) to generate a color product, whose absorbance at 412 nm was quantified by a microplate reader (Tecan M200 PRO; Tecan Company, Switzerland). The density of grafted peptides was obtained by a calibration curve constructed under the same test conditions with different concentrations of peptides.

2.3. SCs experiment

The Sprague Dawley rat SCs were ordered from the Cell Bank of Typical Culture Collection of Chinese Academy of Sciences (Shanghai, China), and being cultured in high-glucose Dulbecco's Modified Eagle's Medium (DMEM, Gibco, USA), which was supplemented with 10% (v/v) fetal bovine serum (FBS, Sijiqing Inc., Hangzhou, China), 100 μg/mL streptomycin and 100 U/mL penicillin.

All the samples were sterilized with 75% ethanol. After washed with PBS, they were seeded with SCs (2×10^4 cells/cm^2), and were observed by SEM 12 h later [17]. The adhesion SCs number on PLCL films was calculated based on the photos taken by a fluorescence microscope (IX81, Olympus, Japan) [17]. The elongated SCs was measured using the Image Pro Plus software.

The migration of SCs was determined according to the method reported previously [16]. Briefly, 1×10^4 cells/cm^2 SCs were seeded on each film, which was placed in a small incubation chamber and observed *in situ* by a time-lapse phase-contrast microscope (DMI6000B, Leica). The reconstructed trajectories, migration distance and rate of SCs were obtained by NIH Image J software and Chemotaxis Tool (Ibidi, Germany). The migration rates in parallel ($V_{//}$) directions, and the net displacement of SCs were calculated respectively.

2.4. Animal investigations

150 Sprague-Dawley rats (200–220 g) were divided into 5 groups. All the animal experimental procedures were guided under Institutional Animal Care guidelines and approved ethically by the Animal Ethics Committee of Hangzhou Medical College (Approval number ZJCLA-IACUC-20010010). The PLCL nerve guidance conduits (NGCs) with a diameter of 1.5 mm, 12 mm in length and 0.2 mm in the wall thickness were obtained by reeling onto a stainless steel bar and sealing with 8–0 nylon monofilament. The nano indentation apparatus (piuma, OPTICS11 BV, Netherlands) was used to measure the elastic modulus of various films. The NGCs were sutured with the two stumps of a 10 mm gap which was left in the sciatic nerve after 6 mm nerve segment removed. The autograft was carried out by suturing the resected nerve with the lesion after rotated 180°.

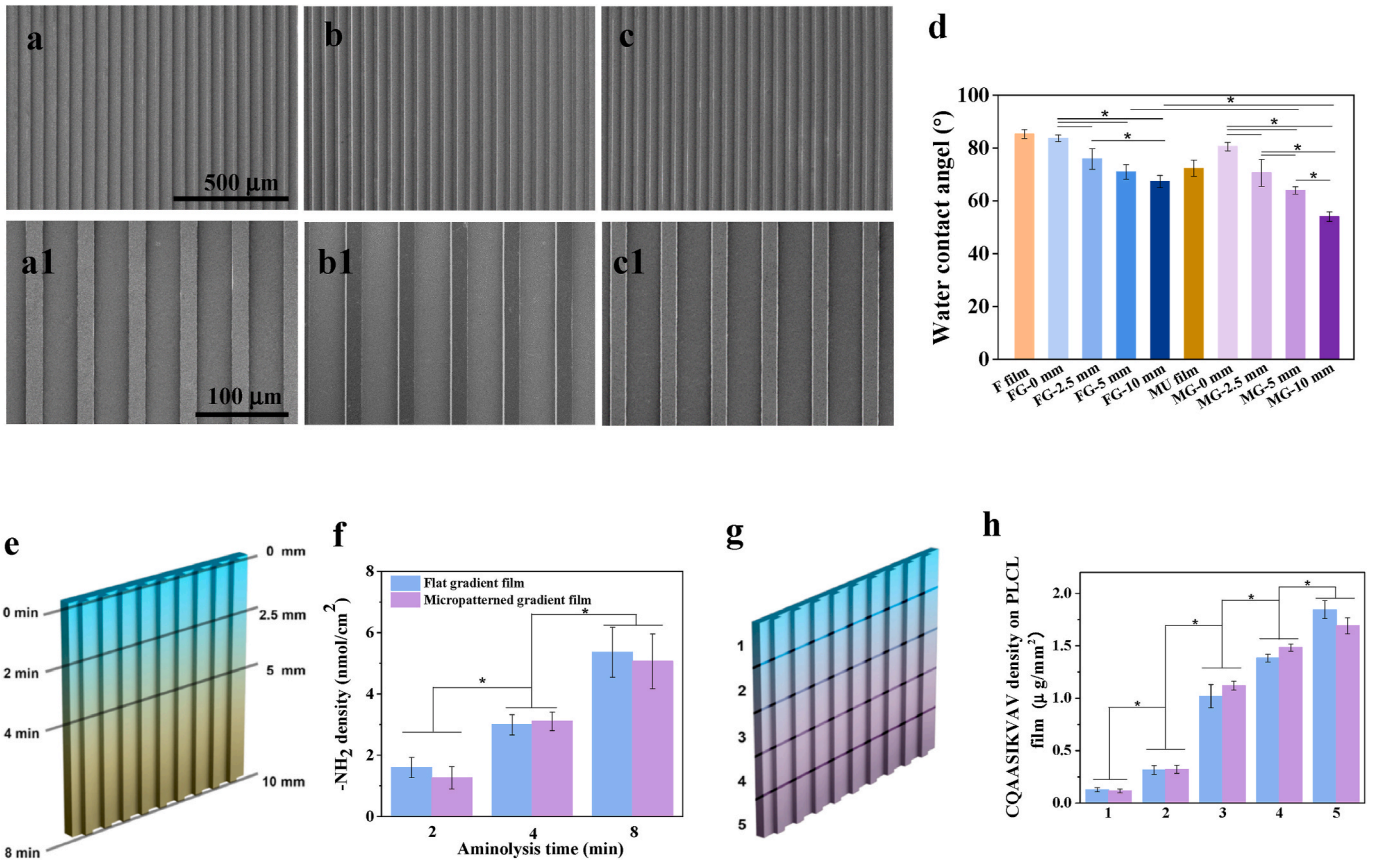

Fig. 1. SEM images of micropatterned PLCL films after being aminolyzed for (a,a1) 2, (b,b1) 4 and (c,c1) 8 min, followed by peptides grafting. (a1-c1) are higher resolution images. (d) Static water contact angles of various films. Due to the anisotropic nature of the micropatterned and/or gradient surfaces, the water contact angles were unsymmetric at different directions and they were detected paralleling to the stripes. (e) Scheme to show the relationship between the aminolysis time and the position of PLCL film. (f) The $-NH_2$ density on the surfaces of flat gradient PLCL and micropatterned gradient PLCL films with various aminolysis time. (g) Scheme to show the five parts of flat gradient PLCL and micropatterned gradient PLCL films for peptide detection. (h) The peptide density on the surface of various micropatterned gradient PLCL position. In this Fig. and thereafter, "F" and "MU" represent the original flat film and the micropatterned PLCL film with uniform peptide density, respectively. The "X" in the FG-X and MG-X (X = 0, 2.5, 5, 10) means the position on the flat and micropatterned PLCL films with a peptide gradient density. * indicates statistically significant difference at $p < 0.05$ level, $n = 4$.

2.4.1. Electrophysiological evaluation

8 and 16 w post-surgery, the sciatic nerve was carefully exposed to detect the nerve conduction velocity (NCV) and compound motor action potential (CMAP). The bipolar stimulating electrodes were used to stimulate the regenerated nerves and the monopolar recording electrode was inserted into the muscle to record electrical activity by a digital MYTO electromyograph machine (Esaote, Genoa, Italy).

2.4.2. Muscle evaluation

Evaluation of wet weight ratio and morphology of muscle: The wet weight ratio (%) of muscles (the wet weight of muscle on the injured side/the wet weight of muscle on the uninjured side × 100%) was determined after the gastrocnemius muscles were harvested at 9 d, 14 d, 8 w and 16 w post-operation, respectively. After immersed in formalin for 1 w, the gastrocnemius muscles were embedded by paraffin for hematoxylin-eosin (HE) before Masson staining. The percentage of collagen fibers was calculated based on the Masson slice images by Image J software.

2.4.3. Investigation of regenerated nerve

The immunofluorescence staining and morphological observation of the regenerated nerves were performed post surgery for 9 d, 14 d, 8 w and 16 w. The proximal segments of 5 regenerated nerves per group after 9 and 14 d implantation were isolated. After fixed in formalin for 3 d, they were embedded by paraffin for immunofluorescence staining of NF200 (mouse anti-rat, 1:500; Peprotech Co., UK), S100β (rabbit anti-rat, 1:500; Peprotech Co., UK), CD86 (mouse anti-rat, 1:500; Peprotech Co., UK), CD163 (rabbit anti-rat, 1:500; Peprotech Co., UK) and DAPI.

After 8 and 16 w implantation, the microstructures such as thickness of the myelin layer and myelinated axon diameter of the regenerated nerves were visualized by transmission electron microscopy (TEM, Hitachi Model H-7650, Japan) after a series of treatments including 2.5% GA/PBS solution, 1% osmium tetroxide, ethanol gradient dehydration, epoxy resin, and sliced by ultrathin section (LEICA EM UC7 ultratome, Germany). The ultrathin slices stained with a trypan blue solution were observed by an optical microscope (IX81, Olympus, Japan).

The immunofluorescence staining of NF200 (mouse anti-rat, 1:500; Peprotech Co., UK), S100β (rabbit anti-rat, 1:500; Peprotech Co., UK) and DAPI in the middle of regenerated nerves after 8 and 16 w implantation were observed by a fluorescence microscope and merged by the Image J software.

Immunohistochemical staining by CD31 antibody (1:150, Abcam, USA) and immunofluorescent staining by rabbit anti-CD34 antibody (1:100, Abcam, USA) were used to assay the angiogenesis of the regenerated nerves, respectively. The positive CD31 area fraction and vessel-like structure (VLS) number/ROI mm^2 were semi-quantified from the CD31 and CD34 images by the Image J software, respectively.

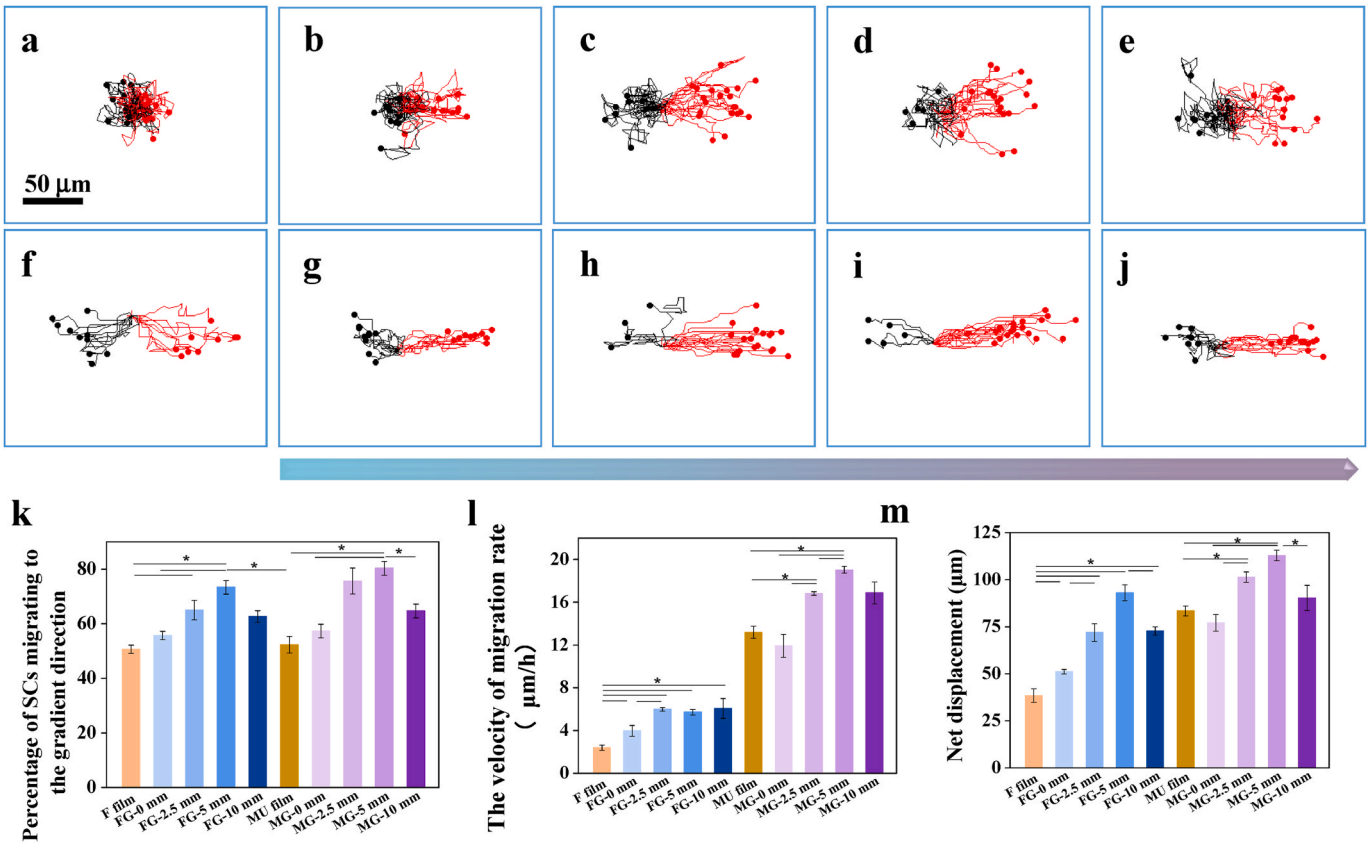

Fig. 2. Migration of single Schwann cell. Migration traces of SCs after being seeded for 12 h at different positions on (a) flat, (b) FG-0, (c) FG-2.5, (d) FG-5, (e) FG-10, (f) MU, (g) MG-0, (h) MG-2.5, (i) MG-5, and (j) MG-10 films, respectively. (k) The statistic percentage of SCs migrating to the gradient direction, (l) migration rates parallel to the gradient direction, and (m) net displacement of SCs quantified from the migration traces. * indicates statistically significant difference at $p < 0.05$ level, $n = 3$.

2.5. Statistical analysis

The data are presented as mean ± standard deviation (SD). Statistical difference is analyzed by one-way analysis of variance (ANOVA) using a Turkey Posthoc method in the Origin 8.5 software. The level of significant difference is set as $p < 0.05$ and $p < 0.01$.

3. Results and discussion

3.1. Fabrication and characterization of micropatterned PLCL films having a peptide density gradient

The cell-substrate interactions take a decisive function on the performance of implantable biomaterials in both the cellular and tissue levels, leading to the difference in tissue regeneration and remodeling *in vivo* [25,26]. In particular, topographical features or the gradient density of biomolecules on a surface can significantly regulate cytoskeleton organization, cell migration, and differentiation of various stem cells [27–29]. For example, the neurites of hippocampal neurons stretched out along the aligned nanofiber of IKVAV-based peptides [30]. A larger number of PC 12 cells adhered on the region of a higher density of IKVAV gradient on poly (ε-caprolactone) fibers [31]. However, the combination of physical guidance and chemical gradient as well as its synergistic effect on tissue repair and regeneration has not been explored so far [32–34]. In this study, for the first time laminin-derived functional CQAASIKVAV peptides were covalently grafted onto micropatterned PLCL films in a gradient manner for conducting various cellular behaviors *in vitro* and enhancing the sciatic nerve regeneration *in vivo* (Scheme 1).

By thermo-pressing a PDMS stamp onto a PLCL film at 190 °C, following with peeling off the stamp after cooling, the linear micropatterns with ridges/grooves width of 20/40 μm were successfully obtained (Figs. S1d and e). The topographical features without noticeable flaws are exactly the replica of the PDMS stamp with ridges/grooves width (40/20 μm) (Figs. S1a–c). The depth of the grooves was maintained at approximately 10 μm without significant difference between each other (Fig. S1f). As a comparison, the flat film without noticeable flaws showed no patterned features (Figs. S1g and h).

In order to find the valid range of peptide density distribution, the micropatterned PLCL film was firstly aminolyzed for various time and then grafted with CQAASIKVAV peptides via GA coupling. The CQAASIKVAV peptide was originated from the effective fragments of laminin, which is validated to enhance the adhesion of SCs and neurite differentiation of PC 12 and DRG cells [35–37]. The number of SCs increased along with the extension of aminolysis until 8 min, and kept unchanged at still longer aminolysis time (Fig. S2). Therefore, the whole aminolysis time to prepare the amino gradient was fixed as 8 min by an injection pump. For the ease of characterization, five representative points at 0, 2, 4 and 8 min, which correspond to the respective positions of 0, 2.5, 5 and 10 mm, were selected. SEM observation (Fig. 1a–c) showed that no significant changes displayed with respect to the overall observation of the linear micropatterns after being treated with various aminolysis time and peptide grafting compared to the original ones (Figs. S1d and e). The well maintained regular stripe morphology suggests that this treatment method is relatively mild and can be generalized for the modification of other types of surface structures. The flat PLCL film, the flat PLCL film with a peptide gradient density, the micropatterned PLCL film with a uniform peptide density (0.84 ± 0.29 μg/mm^2, corresponding to 4 min position) and the micropatterned PLCL film with a peptide gradient density were designated as Flat film, FG film, MU film and MG film,

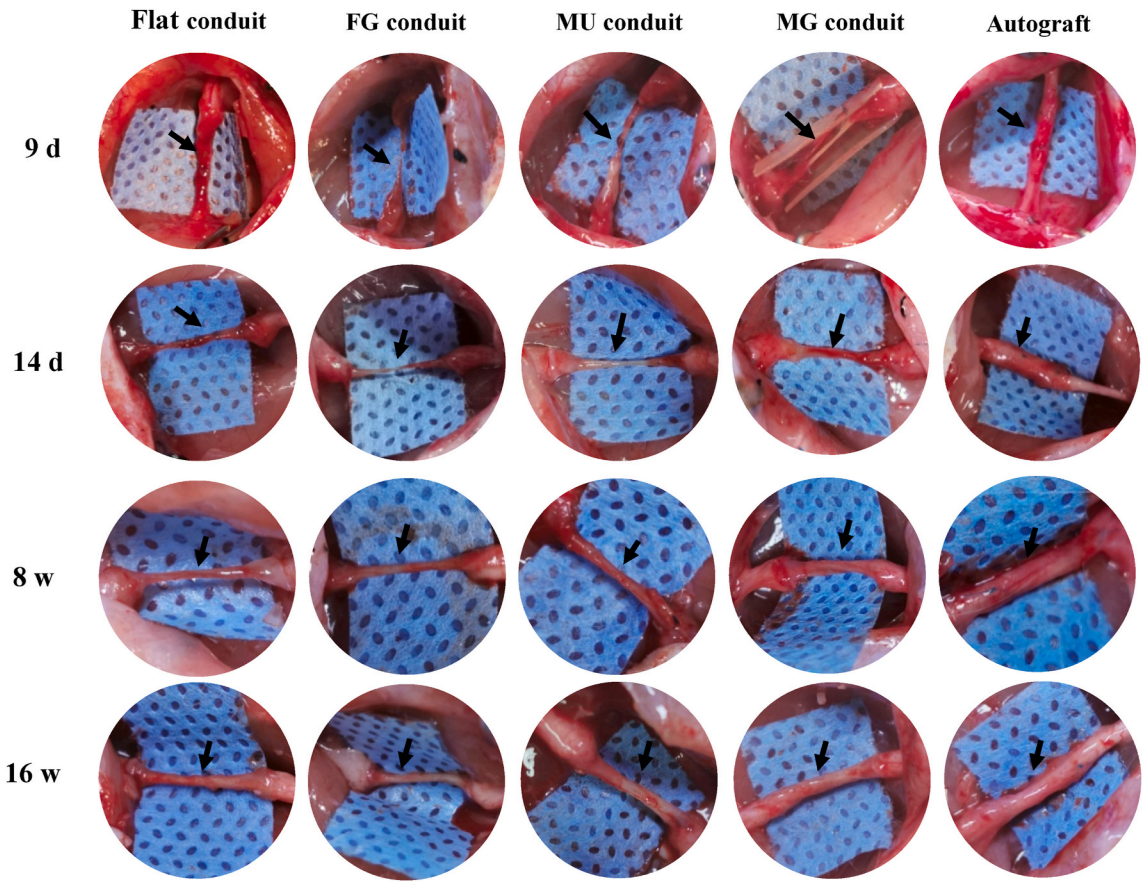

Fig. 3. Optical images of regenerated nerves *in vivo*. The typical photos of regenerated nerves by Flat (the flat PLCL film), FG (the flat PLCL film with a peptide gradient density), MU (the micropatterned PLCL film with uniform peptide density), MG (the micropatterned PLCL film with a peptide gradient density) conduits, and autografts post-surgery for 9 d, 14 d, 8 w and 16 w.

respectively. The various positions on the FG and MG film were designated as FG-number or MG-number.

The surface water contact angles decreased along with the extension of positions (aminolysis time) on both the FG and MG films (Fig. 1d), revealing the gradually enhanced wettability. Comparatively, the MG films were more hydrophilic than the FG films at the same position, e.g. the water contact angle on the FG films decreased from 83.7° to 67.3°, whereas the one on the MG films changed from 80.5° to 54°. This is attributed to the synergetic effect of the stripes, which limit the water drop in an oval shape along the microgrooves [17]. Moreover, a water droplet with unsymmetrical shape on the gradient surface as shown in Fig. S3.

The enhancement of surface wettability must depend on the alteration of chemical structures. The $-NH_2$ density on both the FG and MG films at different positions (Fig. 1e and f) increased significantly along with the prolongation of aminolysis time or position ($p < 0.05$) with values of 1.6, 2.9 and 5.3 $\mu g/cm^2$ after 2, 4 and 8 min aminolysis regardless of the surface topography, respectively. The peptide density was quantified by referring to a calibration curve (Fig. S4), showing a similar alteration tendency on both the FG and MG films (Fig. 1g and h). These results are consistent with the surface wettability, and confirm also the gradient distribution of peptides on the obtained films.

3.2. Adhesion and migration of SCs in vitro

In PNS SCs are the dominant glia cells that form the guidance lines to induce axon sprout and head to the distal stump after nerve injury [38]. Therefore, directional migration of SCs acts positively in filling the nerve gap and accelerating the nerve repair [39]. In this study, migration of single SCs was characterized to explore the guidance effect of the micropatterned and/or gradient substrates. SEM observation (Figs. S5a–j) shows that the SCs are elliptic or fan-shaped on Flat PLCL film and FG-0 mm with a few lamellipodia and filopodia (Figs. S5a and b). On the peptide gradient FG film (Figs. S5c–e), especially on the FG-10 mm position, long neurite-like fibers were formed. When being attached to the ridges, spindle or oval-like shape SCs were observed due to the contact guidance effect from the micropatterned PLCL films (Figs. S5f–j). On the MU film (Fig. S5f), the SCs were drastically elongated along the patterns, presenting protruding neurite-like appearance. The SCs showed more organized filopodia and lamellipodia as the density of peptides increased (Figs. S5g–j).

The adhesion number of SCs increased as the peptide density increased on both the FG and MG films (Fig. S5k). In order to minimize the irregular misconnection during the nerve regeneration process, it is preferable for SCs to elongate and orientate and thereby to lead the axon direction [40]. Therefore, the elongation of SCs is an important index to reflect polarization and actin orientation of SCs. Fig. S5l shows that a larger number of SCs were elongated on the positions with higher peptide densities on the FG and MG films. The MG surface showed a synergistic effect, resulting in significantly higher percentage of elongated cells at the same peptide density positions ($p < 0.05$).

The migration of a single SC on various substrates was then monitored dynamically using a time-lapse microscope. The offset trajectory was normalized to the original position (0,0) in the x-y plane (Fig. 2a–j) for the ease of comparison. The SCs showed no preferred orientation on the Flat films (Fig. 2a) while toward to the direction of higher peptide density on the FG film (Fig. 2b–e). Differently, on all the micropatterned surfaces (Fig. 2f–j) the SCs migrated directionally along the stripe

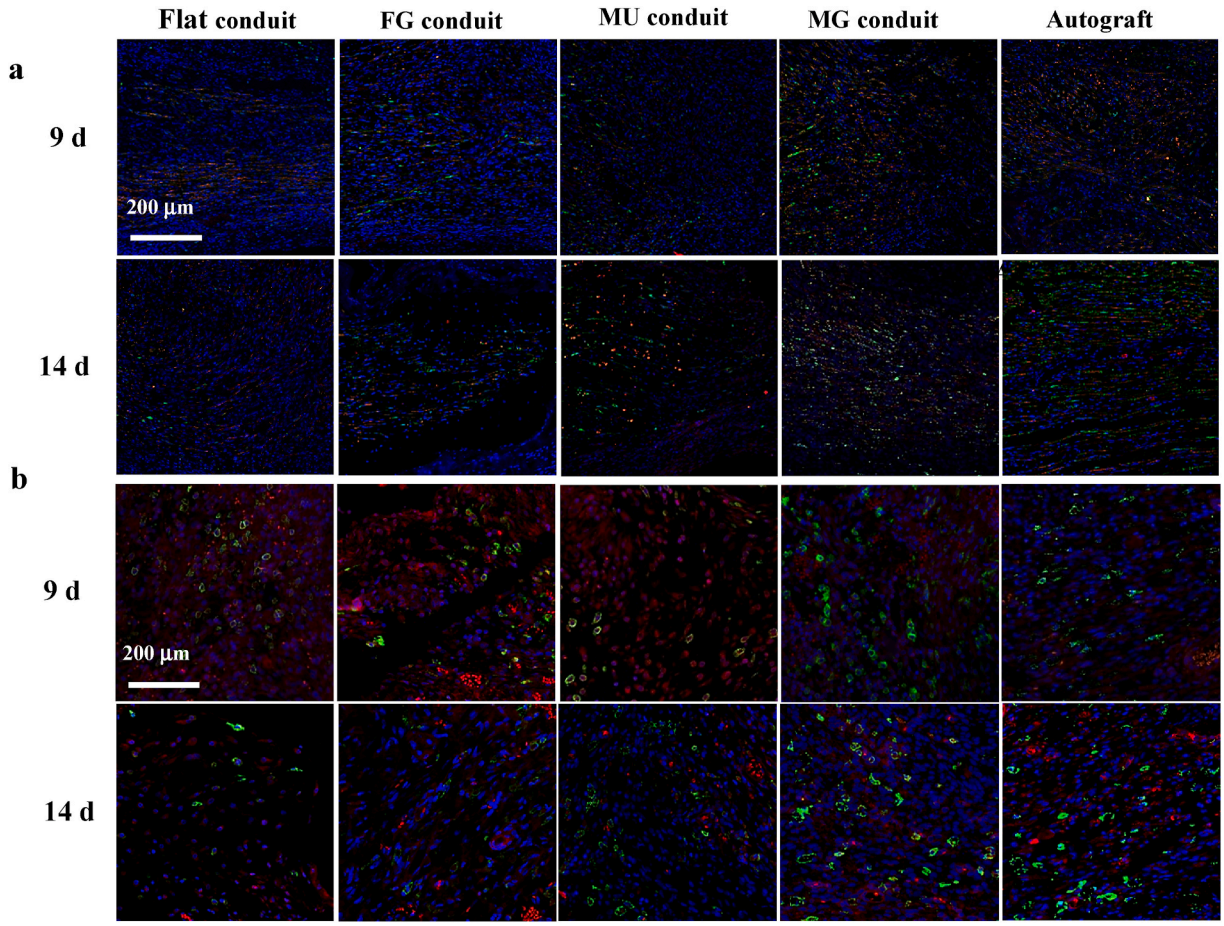

Fig. 4. (a) Merged immunofluorescence staining images of S100β (green), NF200 (red), and DAPI (blue) for SCs, axons and cell nuclei in proximal parts of newborn nerves post surgery for 9 and 14 d, respectively. (b) Merged immunofluorescence staining images of CD163 (green), CD86 (red), and DAPI (blue) for M2, M1 and cell nuclei in the proximal segments of regenerated nerves post surgery for 9 and 14 d, respectively. (For interpretation of the references to color in this figure legend, the reader is referred to the Web version of this article.)

direction, whereas preferably headed to the direction of higher peptide density on the MG film (Fig. 2g–j). Statistical analysis confirmed more quantitatively this observation (Fig. 2k), where the highest percentage about 80% was achieved at the 5 mm position ($p < 0.05$). To facilitate analysis, the velocity was decoupled in the parallel ($\nu_{//}$) and perpendicular directions ($\nu_{\perp}$) to the gradient and micropatterned direction, and the $\nu_{//}$was defined as the valid migration rate [16]. The $\nu_{||}$ rate of SCs (Fig. 2I) was remarkably promoted on the peptides-grafted films compared to the Flat control ($p < 0.05$), and became more significantly faster on the micropatterned PLCL films (all>11 μm/h) decorated with gradient peptides ($p < 0.05$). Moreover, the values on the positions of higher peptide densities were larger than those of lower peptide densities ($p < 0.05$). These results are consistent with the high percentage of SCs being aligned along the micropattern direction (Fig. 2k). The net displacement (Fig. 2m) is consistent with the $\nu_{//}$, where the farthest displacement of 112 μm was discovered on the position of MG-5 mm ($p < 0.05$). This may be attributed to the moderate slope of peptide density at MG-5mm position, providing the largest unbalanced driving force to accelerate the cellular migration [41].

3.3. Nerve regeneration in vivo

Although several studies have shown the improvement of cellular behaviors controlled by biochemical gradients or physical cues *in vitro*, their effect on promoting the regeneration of nerve *in vivo* has rarely been clarified [42,43]. In this study, to compare the performance of nerve regeneration *in vivo*, the Flat conduit (negative control), FG conduit, MU conduit and MG conduit were prepared, respectively. The elastic modulus on various surfaces was all around 97 ± 4.5 MPa, which was robust to resist compressional collapse and thereby support the regeneration of nerve fibers. The conduits were sutured to bridge the 10 mm gap in rat sciatic nerve for short term (9 and 14 d) and long term (8 and 16 w) to reveal the earlier nerve extension and the functional recovery of the newborn nerves, respectively. Usually the short term studies are used to reveal the possible mechanisms of materials because the earlier materials/cells interactions take a key role for the long term tissue regeneration. The long term studies are mandatory to reveal the regeneration results and functional recovery.

After implantation for 9 d only, the nerves (black arrow pointed out) had already been regenerated in the MG conduit crossing the whole gaps and bridging the two injured stumps, while tissue edema occurred or defects were still remained in other conduit groups (Fig. 3). At 14 d post surgery, the regenerated nerves bridged the injury ends in all groups, and that in the MG group showed much brawnier than others. The regenerated nerves in all groups became much stouter after 8 and 16 w implantation.

The immunofluorescence staining in Fig. 4a reveals larger numbers of SCs (green) and axon (red) in the MG group, suggesting better regeneration performance than others at the earlier stage (9 and 14 d). After nerve injury, macrophages will migrate into the wound regions to phagocytize and clean up debris [44,45]. They can be differentiated into M1 or M2 phenotypes, regulating inflammatory balance and thereby affecting nerve repair [46]. In general, the M2 phenotype promotes normal tissue regeneration, while the persistence of the M1 phenotype

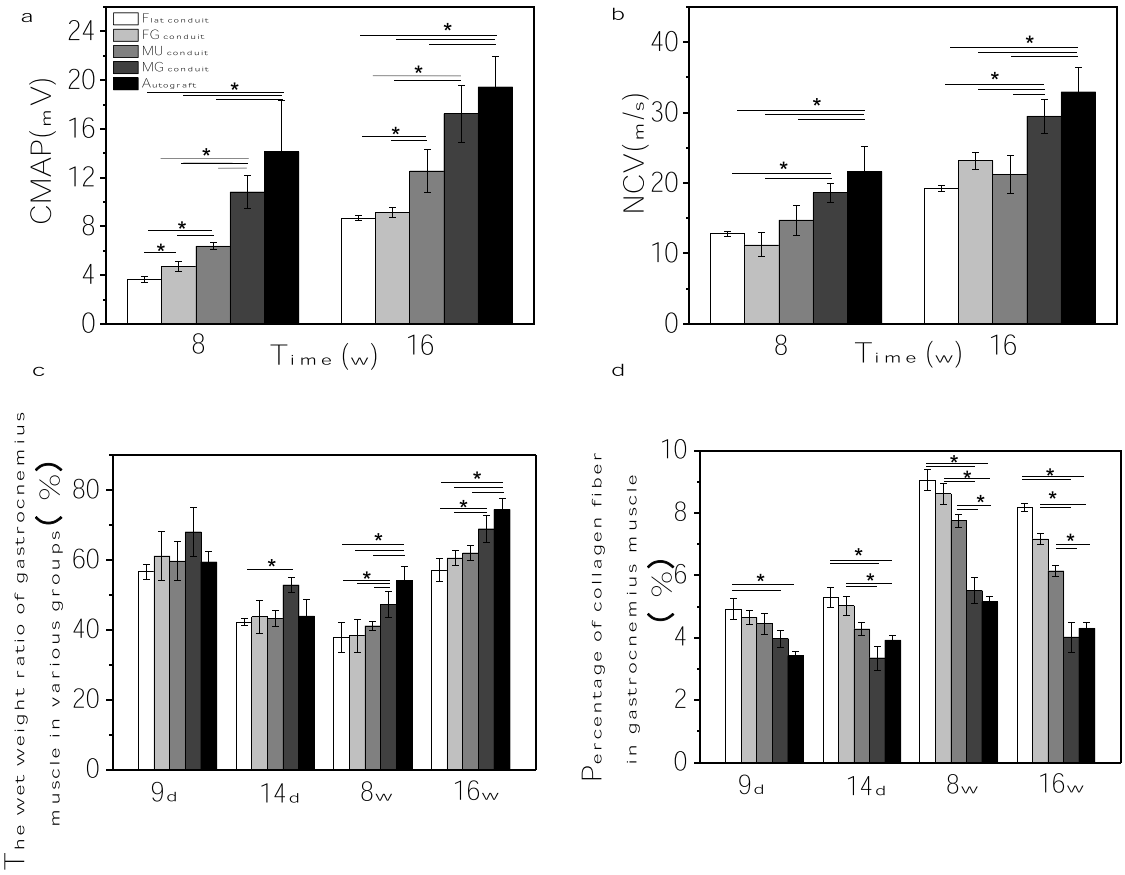

Fig. 5. *In vivo* nerve regenration assay. (a) CMAP amplitude and (b) NCV of regenerated nerves post surgery for 8 and 16 w. (c) Wet weight ratio, (d) percentage of collagen fibers of the gastrocnemius muscles post surgery for 9 d, 14 d, 8 w and 16 w. * indicates statistically significant difference at $p < 0.05$ level, $n = 5$.

may cause tissue fibrosis [47]. Importantly, in the MG group, a larger number of macrophages were polarized to the M2 phenotype, as marked by the CD 163 staining with green color (Fig. 4b), indicating a better microenvironment for nerve regeneration compared with other groups at the earlier stage too.

To measure the functional recovery of the regenerated sciatic nerves, the nerve conduction velocity (NCV) and compound motor action potential (CMAP) were quantified under anesthesia. The CMAP amplitudes increased with the extension of implantation time in all animal groups, and improved with the sequence of Flat, FG, MU, MG and Autograft (Fig. 5a). However, the values in the MG conduit group (~10.8 mV and~17.2 mV at 8 and 16 w, respectively) were obviously larger than those in all the other PLCL groups, approximating those in autograft group (~14.1 mV and~19.4 mV) as well. The variation trend of NCV in different groups was similar to that of CMAP at 8 and 16 w (Fig. 5b). Again, the NCV value of MG group was apparently higher than those of other PLCL groups ($p < 0.05$) at 16 w, which approached to the value of the autograft group too.

As the morphology and function target muscles were deeply administrated by the motor nerves, the wet weight ratio of muscles between the injured and uninjured sides was a vital indicator to reflect the muscle amyotrophy. Fig. 5c shows that the muscle ratio decreased at 14 d and 8 w compared to that at 9 d among all the groups, which then increased 16 w later. Nonetheless, the ratio of MG group (69 ± 3.9%) was comparatively higher than those of the other PLCL groups ($p < 0.05$) at 16 w, which was close to that of the Autograft group (74.5 ± 3.1%).

The percentage of collagen fiber is an indicator for the fibrosis in the muscle tissue. The statistical results (Fig. 5d) semi-quantified from Figs. S6–9 show that less collagen fibers were formed in the MG group compared with other PLCL groups at all time points ($p < 0.05$), which showed no obvious difference with the Autograft control, suggesting less fibrosis and better recovery of muscles in the MG group.

The electrophysiological and muscular atrophy assessment proves that the regenerated nerve function was partially restored in each group, but the exact degrees were different. The reconstruction must lie on the inner microstructure of newborn nerves including the myelinated nerve fibers and regenerated blood vessels [16]. The S100β, NF200 and DAPI staining was performed to reveal the SCs, axon and cell nuclei, respectively. SCs are one of the main components of myelin sheath, and hence could also be used to indicate the myelin sheath. The expression of abundant S100β and NF200 were found in all the newborn nerves post surgery for 16 w (Fig. 6a–e). The white arrows point the axon fibers wrapped by SCs in the regenerated nerves [48,49], demonstrating that plenty of nerve fibers were wrapped by myelin sheath. Again, the MG group possessed the largest number of myelinated nerve fibers (Fig. 6d).

The overall morphology of the newborn nerves was observed by both optical microscopy and TEM. The formation of myelinated nerve axons were proofed by Trypan blue staining in all groups at 8 and 16 w (Fig. S10). The representative TEM images also confirmed the morphological improvement from 8 w to 16 w (Fig. 7a–j), where the statistical results of myelinated axons were consistent with those of the immunofluorescence assay. A larger number of myelinated axons were found in the MG conduit compared with those in the other PLCL groups ($p < 0.05$) at 8 and 16 w (Fig. 7k). Specially, no significant difference was found between the MG conduit and Autograft group at 16 w ($p > 0.05$). Besides, the average myelinated axon diameters and the thickness of myelin sheath of MG group were also highest without significant

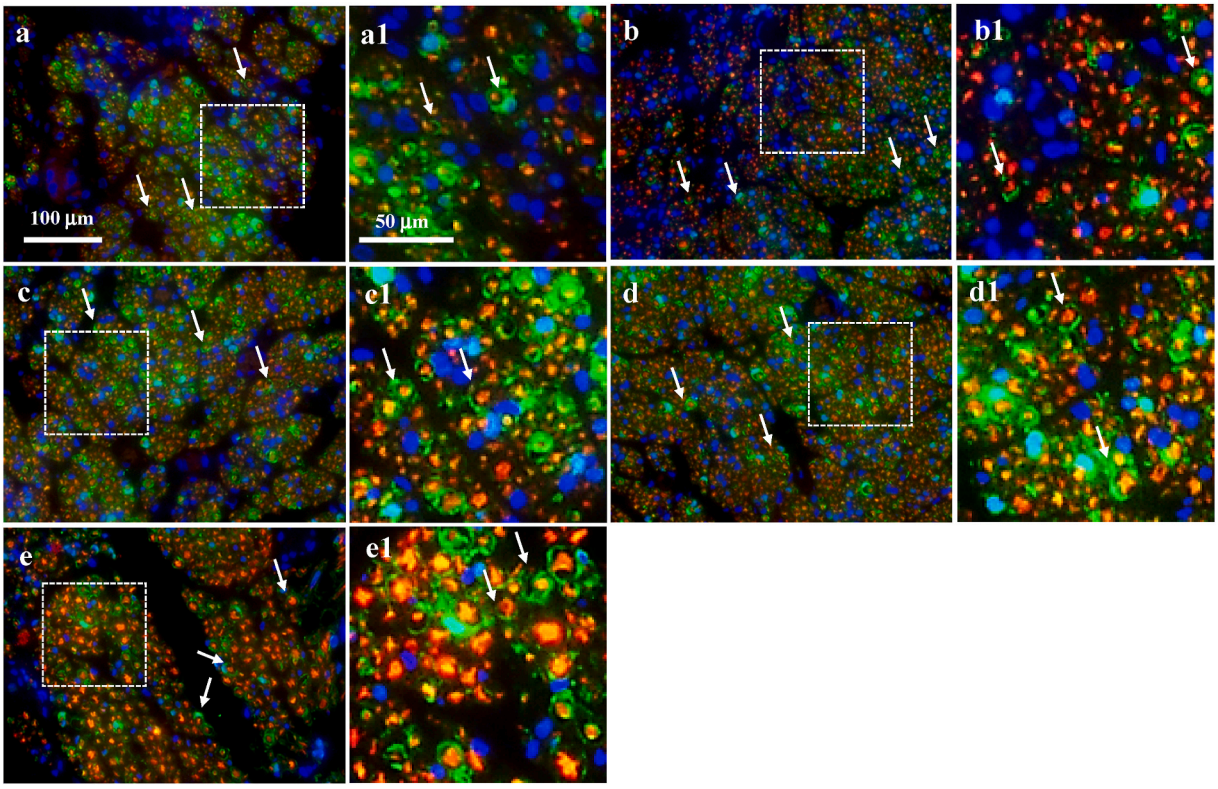

Fig. 6. Microstructures assay *in vivo*. Merged immunofluorescence staining images of green S100β (SCs), red NF200 (axons), and blue DAPI (cell nuclei) of newborn nerves guided by (a,a1) Flat, (b,b1) FG, (c,c1) MU, and (d,d1) MG conduits, and (e,e1) autografts at 16 w post-surgery, respectively. The white arrows point the axon fibers wrapped by myelin sheath in the regenerated nerves. (For interpretation of the references to color in this figure legend, the reader is referred to the Web version of this article.)

difference between the Autograft group at 16 w ($p > 0.05$).

Normally, the blood vessels are always formed accompanying nerves, and the angiogenesis is intrinsically tired with the reinnervation of regenerated nerves [50], because they provide nutrients and oxygen for nerve regeneration. To measure the angiogenesis in newborn nerves, the vascularization-related markers CD31 and CD34 were selected for immunoassay. CD31 is platelet endothelial cell adhesion molecule-1, a transmembrane protein that controls endothelial cell migration and adhesion, and thus is always used to assess the regeneration of various tissues [51]. CD34, a type of hematopoietic transmembrane protein, is closely related to vascular tissue and thus adopted in endothelial cell staining [52]. The large number of CD31 and CD34 suggest that the number of blood vessels in the regenerated nerve is also large. Positive reaction of CD31 (Fig. 8a–j) and CD34 staining (Fig. 8k-t) revealed coordinately angiogenesis in all groups at both 8 and 16 w post surgery. The positive percentage of CD31 area fraction was scientifically larger in the MG group compared with those in the other PLCL groups ($p < 0.05$) at 16 w (Fig. 8u), and was close to that of the Autograft at 16 w ($p > 0.05$). The VLS number/ROI (Fig. 8v) in the MG conduit was obviously higher than those in the other PLCL groups ($p < 0.05$) at 8 w, although it was smaller than that of the Autograft group at 16 w. The positive percentage of CD34 area fraction was also larger in the MG group compared with those in the other PLCL groups ($p < 0.05$) at 16 w (Fig. 8w), while was smaller than that in Autograft group at 16 w.

All these results demonstrate that the combination use of linear micropatterns and gradient CQAASIKVAV peptides can very effectively conduct the directional migration of SCs *in vitro*, and significantly promote peripheral nerve regeneration *in vivo* in terms of regeneration rate, recovery of nerve functions and microstructures, and reduction of fibrosis in muscle tissues. The improvement of the nerve regeneration is likely related with the alleviation of adverse inflammatory microenvironment representing by the larger number of M2 macrophage, and better blood supply revealing by the larger number of blood vessels.

Integration of spatial topography features and biosignals can effectively mediate and improve the interaction between cells and medical devices, which may provide a preferable microenvironment for tissue regeneration [53]. Micropatterns are one of the effective strategies to regulate a variety of cell behaviors including the directional migration of SCs, differentiation of stem cells into nerve-like cells and oriented elongation of axons [38,54,55]. Recently, gradient materials have caused increasing attention due to the better adaption to the physiological native surrounding environment [56–58]. The adhesion, proliferation, differentiation and migration of cells are well regulated by the biochemical or physical gradients, which in turn affect the injured tissue regeneration [59]. However, engineering a specific implant with both the biochemical gradient and microstructure guidance to guide the cell behaviors *in vitro* and achieve the satisfying recovery *in vivo* has rarely been reported [60]. Herein, the stripe micro-features were created on PLCL films by thermo-pressing a PDMS template (Scheme 1). The micropatterned polyester films with a large area can be easily prepared by this method. As reported, neurites of dorsal root ganglia on 40 μm laminin pattern width show a fast outgrowth rate with a highly oriented feature. This size is appropriate to offer sufficient space for neuron growth and to efficiently guide neurite orientation [15]. Moreover, micropatterned biodegradable polyesters with a ridges/grooves width of 20/40 μm clicked with CQAASIKVAV can significantly promote SCs alignment and directional migration, and neurite outgrowth [17]. Based on these results, the micropatterns of 20/40 μm dimensions are recommended when investigating PNS regeneration *in vivo*. CQAASIKVAV peptides derived from the effective linking fragment of laminin can promote the adhesion of various types of cells, in particular those cells of nervous system. It can induce the neurite differentiation of DRG and PC 12 cells, and is thus beneficial for PNS regeneration *in vivo* [31,61]. The density gradient of CQAASIKVAV peptides will affect the adhesion and

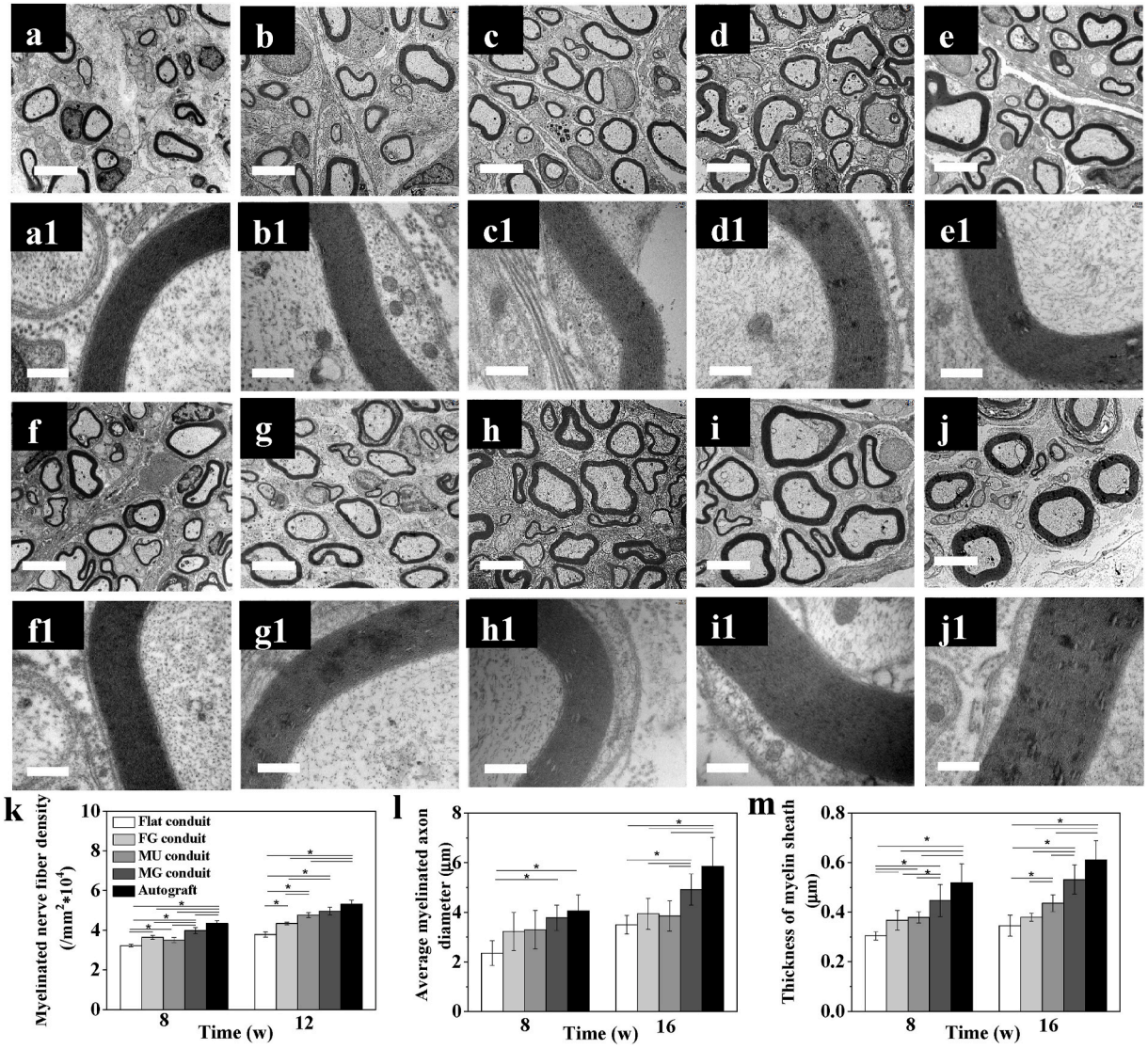

Fig. 7. Microstructures assay *in vivo*. TEM images of newborn nerves guided by (a,a1; f,f1) Flat, (b,b1; g,g1) FG, (c,c1; h,h1) MU, and (d,d1; i,i1) MG conduits, and (e, e1; j,j1) autografts post surgery *in vivo* for (a–e) 8 and (f–j) 16 w, respectively. (k) The number of myelinated axons, (l) average myelinated axon diameter, and (m) thickness of myelin sheath in the middle part of the regenerated nerves post surgery for 8 and 16 w *in vivo*, respectively. The scale bars are 4 μm and 0.4 μm in (a–j) and (a1-j1), respectively. * indicates statistically significant difference at $p < 0.05$ level, $n = 4$.

migration of cells. *In vitro* experiments have proved that when the grafted amount of peptides after 8 min aminolysis of PLCL film may have fully satisfied the binding capacity of receptors on the cell surface. A further increase of the peptide density may exceed the cell's perception of the gradient slope, disabling the effective guidance of the gradient cue.

Although the peptide gradient density was fixed by GA, no obvious cellular and biological toxicity exhibited due to its very tiny amount on the superficial layer, where most aldehyde groups are supposed to be consumed too. GA is also commonly used as a cross-linking agent to prepare tissue regeneration scaffolds. A GA-cross-linked sericin nerve guidance conduit incorporated with clobetasol was fabricated for repairing a 1 cm long sciatic nerve gap in a rat model [62]. Electrospun collagen-chitosan thermoplastic polyurethane nanofibrous scaffolds crosslinked by GA vapor are used as tissue engineered tubular grafts too [63]. The biodegradable PLCL is a commonly used biomedical and tissue regeneration material with good biocompatibility [64]. Moreover, the aminolysis and GA coupling has been extensively used to immobilize different types of molecules on PCL and polylactide surfaces, without any sign of cytotoxicity. Although micro-printing, micro-channels, and 3D printing have been used to prepare gradient biomaterials successfully, these methods cannot be applied on surfaces with topological topography [65]. The construction of gradient polypeptides or factors on oriented surface could be realized by electrospinning or melt spinning, but it is difficult to obtain well precisely repeated parallel samples due to the less controllability of the fabrication processes.

Our gradient aminolysis is inexpensive, and the process is precisely controlled to generate a well distributed $-NH_2$ density gradient on the micropatterned PLCL, which can be then derived into different types of gradients such as proteins, cell growth factors, polysaccharides and drugs besides the peptides demonstrated in this study [66–68]. The manufacture of the multifunctional conduits is feasible by a routine reeling and suturing method. The diameter and length of the guidance conduit can also be easily customized according to the size and position of the injury site.

The SCs tended to elongate along the direction of peptide gradient and micropatterns, benefiting the directional migration (Fig. 2). A previous study shows that the regeneration of peripheral nerve can be enhanced by an asymmetrically porous conduit having an NGF gradient [22], although the functional recovery still needs to improve. The

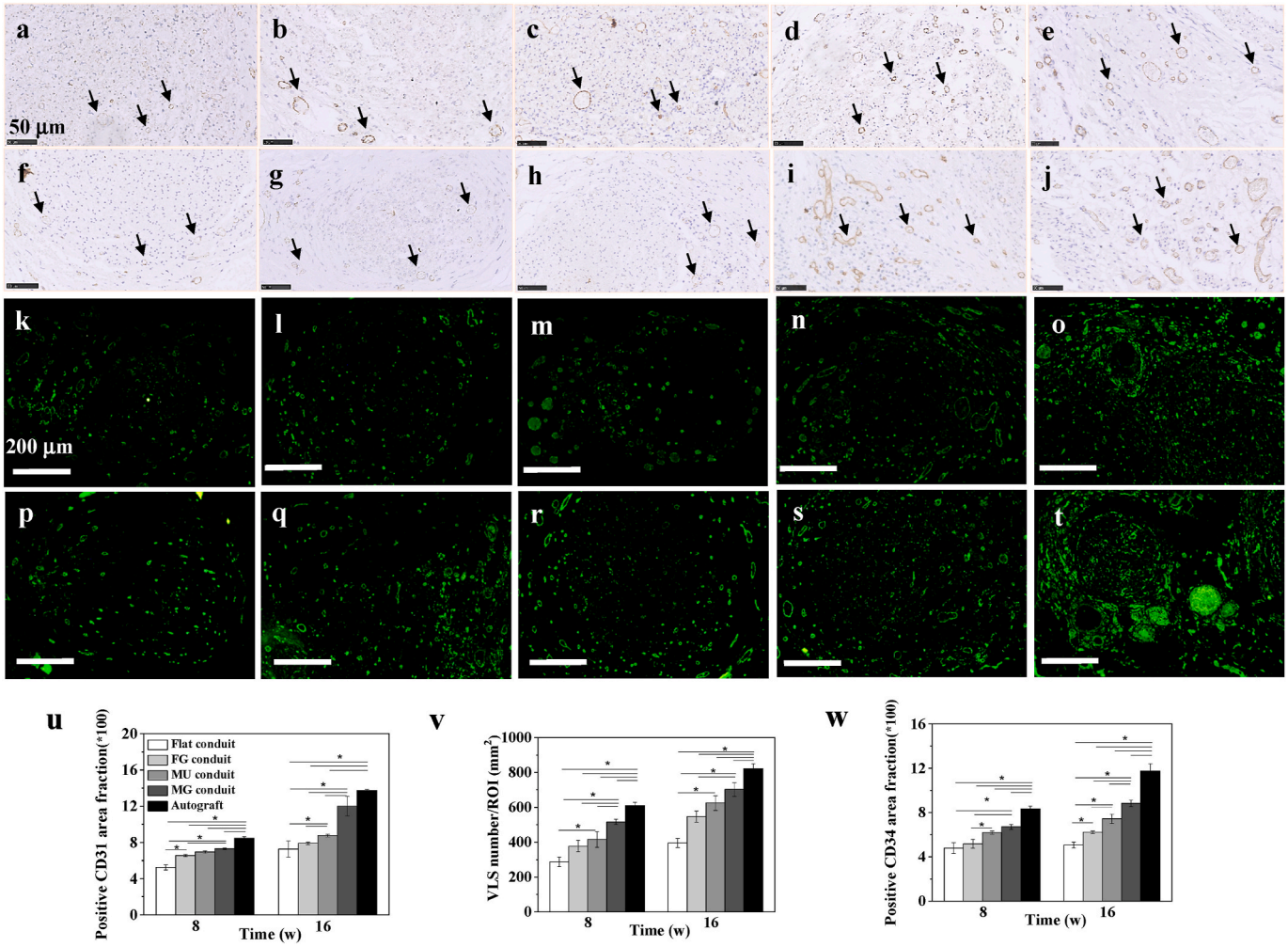

Fig. 8. Vascularization assay *in vivo*. Immunohistochemistry staining for (a–j) CD31 (brown) and nuclei (blue) of newborn nerves guided by (a,f) Flat, (b,g) FG, (c,h) MU, and (d,i) MG conduits, and (e,j) autografts post surgery *in vivo* for 8 (a–e) and 16 (f–j) w, respectively. The black arrows point the vessel-like structure in the regenerated nerves. Immunofluorescence staining for (k–t) CD34 of newborn nerves guided by (k,p) Flat, (l,q) FG, (m,r) MU, and (n,s) MG conduits, and (o,t) autografts post surgery *in vivo* for 8 (k–o) and 16 (p–t) w, respectively. The quantification of (u) positive CD31 area fraction, (v) vessel like structure (VLS) number/ROI mm^2 and (w) positive CD34 area fraction in the middle parts of the regenerated nerves post surgery for 8 and 16 w *in vivo*, respectively. * indicates statistically significant difference at $p < 0.05$ level, $n = 4$. (For interpretation of the references to color in this figure legend, the reader is referred to the Web version of this article.)

frustrated gradient as a result of uncontrolled diffusion of NGF, and the lack of physical guidance effect in the cellular level could be the main reasons. It is assumed that on our micropatterned surface with a covalently grafted peptide gradient the distal end with a higher peptide density is beneficial to the proliferation of SCs, which secret more NGF and other biological factors to induce the axon elongation from the proximal stump to the distal stump. Meanwhile, the stripe micropatterns can guide the regular extension of neurite toward the distal end, both promoting the nerve regeneration with a faster rate and better quality [66]. It is reported that the oriented guidance has a certain regulatory effect on the migration and physiological functions of endothelial cells and smooth muscle cells, and thereby contributing to angiogenesis (Fig. 8) [69]. Besides, the attachment of endothelial cells and smooth muscle cells could be enhanced by the IKVAV sequence, which is derived from the active fragment of laminin [70,71]. Consequently, the micropatterns and peptide gradient can also facilitate the formation of blood vessels and further promote nerve regeneration. For instance, in sprouting angiogenesis, endothelial cells are required to orientate in the tissue environment in order to effectively invade tissues and form vascular patterns [72]. During nerve regeneration, the regenerated nerves provide signals and nutrients to the innervated muscles, and prevent muscle from further atrophy and fibrosis, reducing the content of collagen deposition [73]. The microenvironment of tissue regeneration involves a variety of cells, factors, inorganic ions, etc., and is very complex. The phenotypic changes of macrophages are one of the factors that affect the microenvironment. Meanwhile, the stripe structure is also conducive to physically guiding macrophages to undergo phenotypic differentiation and secrete anti-inflammatory factors. The micropatterns and polypeptide gradient may play a regulatory role on multiple types of cells in the process of nerve regeneration including directional migration of SCs, gradient of NGF, orientation elongation of nerve axons, induced M2 macrophage polarization, and orientation and enhanced attachment of cells related to angiogenesis, which contribute to form a beneficial microenvironment for nerve regeneration. Changes in cell behaviors also affect its own factor secretion, thereby affecting the microenvironment of nerve regeneration. Although our experimental results have shown that this material system can provide a relatively good regeneration environment for nerve regeneration, further studies are required to explore the interplay between our micropatterns and peptide gradient and those significant biomolecules and cells, and thereby to clarify more precisely the intrinsic mechanism on nerve regeneration.

This proof-of-concept nerve guidance conduit can thus better mimic

and simulate the microenvironment in contact with cells by a dual guiding effect, which can more easily adapt the physiological conditions. The reconstruction and functional recovery of regenerated nerve by the micropatterned PLCL conduit with a peptide gradient density achieves better results than many other types of conduits prepared from electrospun fibers, conductive materials, and loading with various cells or cell growth factors etc. [32,74,75].

Moreover, this study discloses also the importance of dual physical structures and biological cues in tissue regeneration, which inspires the design of novel scaffolds with desired topographical features and gradient distribution of functional molecules to meet the demands for regeneration of diverse types of tissues.

4. Conclusions

The linear micropatterns on PLCL films modified with a CQAASIKVAV peptide gradient were fabricated. The NGCs with these features could well guide the migration of SCs directionally *in vitro,* and enhance the regeneration of sciatic nerves in rats *in vivo*. The micropatterns were kept unchanged after aminolysis, GA coupling and peptides grafting. The micropatterned PLCL films modified with a CQAASIKVAV peptide gradient could achieve effective migration of SCs directionally. The NGC made from MG film achieved the best regeneration of rat sciatic nerves *in vivo*, whose comprehensive performance was very close or equal to that of the Autografts. This study verifies that the combination of biochemical gradient signal and physical topology can effectively promote tissue regeneration i*n vivo*, and sheds a light to design novel scaffolds with better performance for the repair of diverse types of tissues.

Data availability statement

The raw/processed data forms part of an ongoing study and may be requested from the authors.

Author contributions statement

D. Zhang: Conceptualization, Formal analysis, Investigation, Methodology, Visualization, Writing-original draft, Writing-review & editing. **Z. Li:** Investigation, Visualization. **H. Shi:** Methodology, Visualization. **Y. Yao:** Methodology. Investigation, Visualization. **W. Du:** Investigation. **P. Lu:** Methodology. **K. Liang:** Methodology, Investigation. **L. Hong:** Methodology. **C. Gao:** Conceptualization, Formal analysis, Funding acquisition, Project administration, Resources, Supervision, Writing-review & editing.

CRediT authorship contribution statement

Deteng Zhang: Conceptualization, Formal analysis, Investigation, Methodology, Visualization, Writing – original draft, Writing – review & editing. **Ziming Li:** Investigation, Visualization. **Haifei Shi:** Methodology, Visualization. **Yuejun Yao:** Methodology, Investigation, Visualization. **Wang Du:** Investigation. **Pan Lu:** Methodology. **Kejiong Liang:** Methodology, Investigation. **Liangjie Hong:** Methodology. **Changyou Gao:** Conceptualization, Formal analysis, Funding acquisition, Project administration, Resources, Supervision, Writing – review & editing.

Declaration of competing interest

The authors declare that they have no known competing financial interests or personal relationships that could have appeared to influence the work reported in this paper.

Acknowledgements

This study is financially supported by the National Key Research and Development Program of China (2016YFC1100403), the National Natural Science Foundation of China (21434006, 51873188), and the Fundamental Research Funds for the Central Universities of China (2020XZZX004-01).

Appendix A. Supplementary data

Supplementary data to this article can be found online at https://doi.org/10.1016/j.bioactmat.2021.07.010.

References

[1] A. Leal-Egaña, A. Díaz-Cuenca, A.R. Boccaccini, Tuning of cell-biomaterial anchorage for tissue regeneration, Adv. Mater. 25 (2013) 4049–4057.
[2] X. Shi, Y. Zhao, J. Zhou, S. Chen, H. Wu, One-step generation of engineered drug-laden poly(lactic-co-glycolic acid) micropatterned with Teflon chips for potential application in tendon restoration, ACS Appl. Mater. Interfaces 5 (21) (2013) 10583–10590.
[3] C.H. Kim, G. W Kim, H. Jae, Submicron-patterned fibronectin controls the biological behavior of human dermal fibroblasts, J. Nanosci. Nanotechnol. 10 (10) (2010) 6864–6868.
[4] S.M. Kristyn, S.A. Kristi, Cell–material interactions, Adv. Chem. Eng. 29 (2004) 7–46.
[5] R. Obregón, J. Ramón-Azcón, S. Ahadian, H. Shiku, M. Ramalingam, A. Khademhosseini, T. Matsue, Gradient Biomaterials as Tissue Scaffolds, 2015, pp. 175–186.
[6] E.T. Roussos, J.S. Condeelis, A. Patsialou, Chemotaxis in cancer, Nat. Rev. Canc. 11 (8) (2011) 573–587.
[7] R.K. Paradise, M.J. Whitfield, D.A. Lauffenburger, K.J. Van Vliet, Directional cell migration in an extracellular pH gradient: a model study with an engineered cell line and primary microvascular endothelial cells, Exp. Cell Res. 319 (4) (2013) 487–497.
[8] S. Xin, J. Dai, C.A. Gregory, A. Han, D.L. Alge, Creating physicochemical gradients in modular microporous annealed particle hydrogels via a microfluidic method, Adv. Funct. Mater. 30 (2019) 1907102.
[9] P. Xue, W. Liu, Z. Gu, X. Chen, J. Nan, J. Zhang, H. Sun, Z. Cui, B. Yang, Graded protein/PEG nanopattern arrays well-defined gradient biomaterials to induce basic cellular behaviors, ACS Appl. Mater. Interfaces 11 (1) (2018) 1595–1603.
[10] C. Zink, H. Hall, D.M. Brunette, N.D. Spencer, Orthogonal nanometer-micrometer roughness gradients probe morphological influences on cell behavior, Biomaterials 33 (32) (2012) 8055–8061.
[11] C. Kim, J.L. Young, A.W. Holle, K. Jeong, L.G. Major, J.H. Jeong, Z.M. Aman, D.-W. Han, Y. Hwang, J.P. Spatz, Y.S. Choi, Stem cell mechanosensation on gelatin methacryloyl (GelMA) stiffness gradient hydrogels, Ann. Biomed. Eng. 48 (2) (2019) 893–902.
[12] Y. Hou, W. Xie, L. Yu, L.C. Camacho, C. Nie, M. Zhang, R. Haag, Q. Wei, Surface roughness gradients reveal topography-specific mechanosensitive responses in human mesenchymal stem cells, Small 16 (10) (2020) 1905422.
[13] Y.-W. Won, A.N. Patel, D.A. Bull, Cell surface engineering to enhance mesenchymal stem cell migration toward an SDF-1 gradient, Biomaterials 35 (21) (2014) 5627–5635.
[14] D. Santos, P. Wieringa, L. Moroni, X. Navarro, J.D. Valle, PEOT/PBT guides enhance nerve regeneration in long gap defects, Adv. Health. Mater. 6 (3) (2017) 27973708.
[15] M. Song, K.E. Uhrich, Optimal micropattern dimensions enhance neurite outgrowth rates, lengths, and orientations, Ann. Biomed. Eng. 35 (10) (2007) 1812–1820.
[16] D. Zhang, Y. Yao, Y. Duan, X. Yu, H. Shi, J.R. Nakkala, X. Zuo, L. Hong, Z. Mao, C. Gao, Surface-anchored graphene oxide nanosheets on cell-scale micropatterned poly(d,;l-lactide-co-caprolactone) conduits promote peripheral nerve regeneration, ACS Appl. Mater. Interfaces 12 (7) (2020) 7915–7930.
[17] D. Zhang, S. Wu, J. Feng, Y. Duan, D. Xing, C. Gao, Micropatterned biodegradable polyesters clicked with CQAASIKVAV promote cell alignment, directional migration, and neurite outgrowth, Acta Biomater. 74 (2018) 143–155.
[18] A. Seidi, M. Ramalingam, I. Elloumi-Hannachi, S. Ostrovidov, A. Khademhosseini, Gradient biomaterials for soft-to-hard interface tissue engineering, Acta Biomater. 7 (4) (2011) 1441–1451.
[19] R.I. Sharma, J.G. Snedeker, Biochemical and biomechanical gradients for directed bone marrow stromal cell differentiation toward tendon and bone, Biomaterials 31 (30) (2010) 7695–7704.
[20] T. Ren, S. Yu, Z. Mao, C. Gao, A complementary density gradient of zwitterionic polymer brushes and NCAM peptides for selectively controlling directional migration of Schwann cells, Biomaterials 56 (2015) 58–67.
[21] S. Tang, J. Zhu, Y. Xu, A.P. Xiang, M.H. Jiang, D. Quan, The effects of gradients of nerve growth factor immobilized PCLA scaffolds on neurite outgrowth in vitro and peripheral nerve regeneration in rats, Biomaterials 34 (29) (2013) 7086–7096.
[22] S.H. Oh, J.G. Kang, T.H. Kim, U. Namgung, K.S. Song, B.H. Jeon, J.H. Lee, Enhanced peripheral nerve regeneration through asymmetrically porous nerve guide conduit with nerve growth factor gradient, J. Biomed. Mater. Res. 106 (1) (2018) 52–64.

[23] S.H. Oh, T.H. Kim, J.H. Lee, Creating growth factor gradients in three dimensional porous matrix by centrifugation and surface immobilization, Biomaterials 32 (32) (2011) 8254–8260.
[24] S. Yu, Z. Mao, C. Gao, Preparation of gelatin density gradient on poly(epsilon-caprolactone) membrane and its influence on adhesion and migration of endothelial cells, J. Colloid Interface Sci. 451 (2015) 177–183.
[25] A.P. Acharya, N.V. Dolgova, N.M. Moore, C.-Q. Xia, M.J. Clare-Salzler, M.L. Becker, N.D. Gallant, B.G. Keselowsky, The modulation of dendritic cell integrin binding and activation by RGD-peptide density gradient substrates, Biomaterials 31 (29) (2010) 7444–7454.
[26] Y. Aizawa, R. Wylie, M. Shoichet, Endothelial cell guidance in 3D patterned scaffolds, Adv. Mater. 22 (43) (2010) 4831–4835.
[27] J.P. Alves-Lopes, O. Söder, J.-B. Stukenborg, Use of a three-layer gradient system of cells for rat testicular organoid generation, Nat. Protoc. 13 (2) (2018) 248–259.
[28] T.-a. Asoh, M. Matsusaki, T. Kaneko, M. Akashi, Fabrication of temperature-responsive bending hydrogels with a nanostructured gradient, Adv. Mater. 20 (2008) 2080–2083.
[29] B. Cortese, G. Gigli, M. Riehle, Mechanical gradient cues for guided cell Motility and control of cell behavior on uniform substrates, Adv. Funct. Mater. 19 (2009) 2961–2968.
[30] A. Li, A. Hokugo, A. Yalom, E.J. Berns, N. Stephanopoulos, M.T. McClendon, L. A. Segovia, I. Spigelman, S.I. Stupp, R. Jarrahy, A bioengineered peripheral nerve construct using aligned peptide amphiphile nanofibers, Biomaterials 35 (31) (2014) 8780–8790.
[31] S.E. Kim, E.C. Harker, A.C. De Leon, R.C. Advincula, J.K. Pokorski, Coextruded, aligned and gradient-modified poly(epsilon-caprolactone) fibers as platforms for neural growth, Biomacromolecules 16 (3) (2015) 860–867.
[32] V. Chiono, C. Tonda-Turo, Trends in the design of nerve guidance channels in peripheral nerve tissue engineering, Prog. Neurobiol. 131 (2015) 87–104.
[33] S.Y. Chew, R. Mi, A. Hoke, K.W. Leong, Aligned protein-polymer compositfibers enhance nerve regeneration: a potential tissue-engineering platform, Adv. Funct. Mater. 17 (8) (2007) 1288–1296.
[34] C. Chen, J. Tang, Y. Gu, L. Liu, X. Liu, L. Deng, C. Martins, B. Sarmento, W. Cui, L. Chen, Bioinspired hydrogel electrospun fibers for spinal cord regeneration, Adv. Funct. Mater. 29 (2019) 1806899.
[35] T.B. Aigner, E. DeSimone, T. Scheibel, Biomedical applications of recombinant silk-based materials, Adv. Mater. 30 (19) (2018) 1704636.
[36] L.M. Yu, K. Kazazian, M.S. Shoichet, Peptide surface modification of methacrylamide chitosan for neural tissue engineering applications, J. Biomed. Mater. Res. 82 (1) (2007) 243–255.
[37] L.M.Y. Yu, N.D. Leipzig, M.S. Shoichet, Promoting neuron adhesion and growth, Mater. Today 11 (2008) 6–43.
[38] G. Li, X. Zhao, W. Zhao, L. Zhang, C. Wang, M. Jiang, X. Gu, Y. Yang, Porous chitosan scaffolds with surface micropatterning and inner porosity and their effects on Schwann cells, Biomaterials 35 (30) (2014) 8503–8513.
[39] M.F. Daud, K.C. Pawar, F. Claeyssens, A.J. Ryan, J.W. Haycock, An aligned 3D neuronal-glial co-culture model for peripheral nerve studies, Biomaterials 33 (25) (2012) 5901–5913.
[40] I. Tonazzini, E. Jacchetti, S. Meucci, F. Beltram, M. Cecchini, Schwann cell contact guidance versus boundary-interaction in functional wound healing along nano and microstructured membranes, Adv. Health. Mater. 4 (12) (2015) 1849–1860.
[41] T. Ren, S. Yu, Z. Mao, S.E. Moya, L. Han, C. Gao, Complementary density gradient of Poly(hydroxyethyl methacrylate) and YIGSR selectively guides migration of endotheliocytes, Biomacromolecules 15 (6) (2014) 2256–2264.
[42] R.R. Bhat, B.N. Chaney, J. Rowley, A. Liebmann-Vinson, J. Genzer, Tailoring cell adhesion using surface-grafted polymer gradient assemblies, Adv. Mater. 17 (2005) 2802–2807.
[43] S.A. DeLong, J.J. Moon, J.L. West, Covalently immobilized gradients of bFGF on hydrogel scaffolds for directed cell migration, Biomaterials 26 (16) (2005) 3227–3234.
[44] Y. Miyake, H. Matsumoto, M. Yokoo, K. Miyazawa, N. Kimura, W.A. Tunjung, T. Shimizu, H. Sasada, H. Aso, T. Yamaguchi, E. Sato, Expression and glycosylation with polylactosamine of CD44 antigen on macrophages during follicular atresia in pig ovaries, Biol. Reprod. 74 (3) (2006) 501–510.
[45] L. Fang, L. Chen, B. Lin, L. Han, K. Zhu, Q. Song, Analysis of inflammatory and homeostatic roles of tissue-resident macrophages in the progression of cholesteatoma by RNA-Seq, Immunol. Invest. (2020) 1–13.
[46] R.E. Zigmond, F.D. Echevarria, Macrophage biology in the peripheral nervous system after injury, Prog. Neurobiol. 173 (2019) 102–121.
[47] P. Hu, E.M. McLachlan, Inflammation in sympathetic ganglia proximal to sciatic nerve transection in rats, Neurosci. Lett. 365 (1) (2004) 39–42.
[48] X.J. Yuan, Y.J. Wei, Q. Ao, K. Gong, J.Y. Wang, Q.S. Sun, L. Zhang, Z.C. Zheng, L. Chen, Myelin ultrastructure of sciatic nerve in rat experimental autoimmune neuritis model and its correlation with associated protein expression, Int. J. Clin. Exp. Pathol. 8 (2015) 7849–7858.
[49] N. Hu, H. Wu, C.B. Xue, Y.P. Gong, J. Wu, Z.Q. Xiao, Y.M. Yang, F. Ding, X.S. Gu, Long-term outcome of the repair of 50 mm long median nerve defects in rhesus monkeys with marrow mesenchymal stem cells-containing, chitosan-based tissue engineered nerve grafts, Biomaterials 34 (2013) 100–111.
[50] T. Wang, Y. Zhai, M. Nuzzo, X. Yang, Y. Yang, X. Zhang, Layer-by-layer nanofiber-enabled engineering of biomimetic periosteum for bone repair and reconstruction, Biomaterials 182 (2018) 279–288.
[51] I.-S. Park, C. Mahapatra, J.S. Park, K. Dashnyam, J.-W. Kim, J.C. Ahn, P.-S. Chung, D.S. Yoon, N. Mandakhbayar, R.K. Singh, J.-H. Lee, K.W. Leong, H.-W. Kim, Revascularization and limb salvage following critical limb ischemia by nanoceria-induced Ref-1/APE1-dependent angiogenesis, Biomaterials 242 (2020), 119919.
[52] K. Takayama, Y. Kawakami, Y. Mifune, T. Matsumoto, Y. Tang, J.H. Cummins, N. Greco, R. Kuroda, M. Kurosaka, B. Wang, F.H. Fu, J. Huard, The effect of blocking angiogenesis on anterior cruciate ligament healing following stem cell transplantation, Biomaterials 60 (2015) 9–19.
[53] R.F. Canadas, T. Ren, A.P. Marques, J.M. Oliveira, R.L. Reis, U. Demirci, Biochemical gradients to generate 3D heterotypic-like tissues with isotropic and anisotropic architectures, Adv. Funct. Mater. 28 (2018) 1804148.
[54] B. Delalat, A. Mierczynska, S.R. Ghaemi, A. Cavallaro, F.J. Harding, K. Vasilev, N. H. Voelcker, Materials displaying neural growth factor gradients and applications in neural differentiation of embryoid body cells, Adv. Funct. Mater. 25 (2015) 2737–2744.
[55] A. Higuchi, Q.-D. Ling, Y. Chang, S.-T. Hsu, A. Umezawa, Physical cues of biomaterials guide stem cell differentiation Fate, Chem. Rev. 113 (5) (2013) 3297–3328.
[56] C.P. Addington, J.M. Heffernan, C.S. Millar-Haskell, E.W. Tucker, R.W. Sirianni, S. E. Stabenfeldt, Enhancing neural stem cell response to SDF-1α gradients through hyaluronic acid-laminin hydrogels, Biomaterials 72 (2015) 11–19.
[57] F. Du, H. Wang, W. Zhao, D. Li, D. Kong, J. Yang, Y. Zhang, Gradient nanofibrous chitosan/poly ϵ-caprolactone scaffolds as extracellular microenvironments for vascular tissue engineering, Biomaterials 33 (2012) 762–770.
[58] S.A. Fisher, R.Y. Tam, A. Fokina, M.M. Mahmoodi, M.D. Distefano, M.S. Shoichet, Photo-immobilized EGF chemical gradients differentially impact breast cancer cell invasion and drug response in defined 3D hydrogels, Biomaterials 178 (2018) 751–766.
[59] A.M. Greiner, M. Jäckel, A.C. Scheiwe, D.R. Stamow, T.J. Autenrieth, J. Lahann, C. M. Franz, M. Bastmeyer, Multifunctional polymer scaffolds with adjustable pore size and chemoattractant gradients for studying cell matrix invasion, Biomaterials 35 (2014) 611–619.
[60] O. Jeon, D.S. Alt, S.W. Linderman, E. Alsberg, Biochemical and physical signal gradients in hydrogels to control stem cell behavior, Adv. Mater. 25 (44) (2013) 6366–6372.
[61] A.-S. Mertgen, V.T. Trossmann, A.G. Guex, K. Maniura-Weber, T. Scheibel, M. Rottmar, Multifunctional biomaterials: combining material modification strategies for engineering of cell-contacting surfaces, ACS Appl. Mater. Interfaces 12 (19) (2020) 21342–21367.
[62] L. Zhang, W. Yang, H. Xie, H. Wang, J. Wang, Q. Su, X. Li, Y. Song, G. Wang, L. Wang, Z. Wang, Sericin nerve guidance conduit delivering therapeutically repurposed clobetasol for functional and structural regeneration of transected peripheral nerves, ACS Biomater. Sci. Eng. 5 (3) (2019) 1426–1439.
[63] C. Huang, R. Chen, Q. Ke, Y. Morsi, K. Zhang, X. Mo, Electrospun collagen-chitosan-TPU nanofibrous scaffolds for tissue engineered tubular grafts, Colloids Surf. B Biointerfaces 82 (2) (2011) 307–315.
[64] S. Tielens, H. Declercq, T. Gorski, E. Lippens, E. Schacht, M. Cornelissen, Gelatin-based microcarriers as embryonic stem cell delivery system in bone tissue engineering: an in-vitro study, Biomacromolecules 8 (2007) 825–832.
[65] E.S. Place, N.D. Evans, M.M. Stevens, Complexity in biomaterials for tissue engineering, Nat. Mater. 8 (2009) 457–470.
[66] C.J. Pateman, A.J. Harding, A. Glen, C.S. Taylor, C.R. Christmas, P.P. Robinson, S. Rimmer, F.M. Boissonade, F. Claeyssens, J.W. Haycock, Nerve guides manufactured from photocurable polymers to aid peripheral nerve repair, Biomaterials 49 (2015) 77–89.
[67] L. Zhu, S. Jia, T. Liu, L. Yan, D. Huang, Z. Wang, Aligned PCL fiber conduits immobilized with nerve growth factor gradients enhance and direct sciatic nerve regeneration, Adv. Funct. Mater. 30 (2020) 2002610.
[68] Y.C. Chang, M.H. Chen, S.Y. Liao, H.C. Wu, C.H. Kuan, J.S. Sun, Multichanneled nerve guidance conduit with spatial gradients of neurotrophic factors and oriented nanotopography for repairing the peripheral nervous system, ACS Appl. Mater. Interfaces 9 (43) (2017) 37623–37636.
[69] S.A. Biela, Y. Su, J.P. Spatz, R. Kemkemer, Different sensitivity of human endothelial cells, smooth muscle cells and fibroblasts to topography in the nano-micro range, Acta Biomater. 5 (7) (2009) 2460–2466.
[70] X. Lin, K. Takahashi, Y. Liu, P.O. Zamora, Enhancement of cell attachment and tissue integration by a IKVAV containing multi-domain peptide, BBA - General Subjects 1760 (2006) 1403–1410.
[71] P. Jung, A.K. Nagaraj, E.K. Fox, J.S. Rudra, J.M. Devgun, J.H. Collier, Co-assembling peptides as defined matrices for endothelial cells, Biomaterials 30 (2009) 2400–2410.
[72] H. Gerhardt, C. Betsholtz, How do endothelial cells orientate? EXS 94 (2005) 3–15.
[73] M. Song, K.E. Uhrich, Optimal micropattern dimensions enhance neurite outgrowth rates, lengths, and orientations, Ann. Biomed. Eng. 35 (10) (2007) 1812–1820.
[74] K.H. Zhang, C.Y. Wang, C.Y. Fan, X.M. Mo, Aligned SF/P(LLA-CL)-blended nanofibers encapsulating nerve growth factor for peripheral nerve regeneration, J. Biomed. Mater. Res. 102 (2014) 2680–2691.
[75] X. Gu, F. Ding, Y. Yang, J. Liu, Construction of tissue engineered nerve grafts and their application in peripheral nerve regeneration, Prog. Neurobiol. 93 (2011) 204–230.